

LIF study of mixing in a model of a vein punctured by a cannula

Andreas Borg, Laszlo Fuchs *

Division of Fluid Mechanics, Lund Institute of Technology, Box 118, 221 00 Lund, Sweden

Abstract

Steady flow and mixing in a model of an “arterialized” vein punctured by a cannula as occurs during hemodialysis has been investigated in vitro. The motivation is that a major cause of vascular access dysfunction is the development of venous stenoses. This phenomenon lacks physiological explanation. However, one may attribute this quick process to the chemical content of the dialyzed blood and its flow near the point of infusion. The interest in mixing of chemical compounds in the dialyzed blood supplied through the cannula is, therefore, genuine due to the clinical impacts of haemodialysis. We are interested in understanding the mixing of the two streams; namely, the untreated blood through the vein and the treated blood through the cannula. This mixing affects the local pH, which in turn can affect the solubility of several salts used for dialysis. In addition, since the blood contains molecules of widely different diffusivity properties, the local composition of blood near the point of injection is of interest. The hypothesis is that concentration non-uniformities may lead to undesired chemical or bio-chemical reactions leading to the pathological processes in the region around the needle. The mixing of a high Schmidt number substance in the stream entering from the cannula with the base flow in the vein is studied by laser induced fluorescence (LIF). The investigations are performed for a range of typical Reynolds numbers in the cannula and the vein found during hemodialysis. The study shows complicated mixing patterns around the cannula, and that non-uniformities in the blood persist over long distances for the lower flow rates found in vivo. For the higher flow rates, the flow loses its stability and mixing is enhanced. The nature of this instability is shown, and quantitative data of concentration fluctuations are given. We have further considered the effect of rotating the cannula. This leads to a significant change in the mixing process. The significance of the non-uniformities in mixing of solvents in the blood for the development of venous stenoses should be further studied not only in fluid dynamical terms but also in terms of endothelial (cellular) effects. © 2002 Published by Elsevier Science Inc.

1. Introduction

The study of flow in large vessels of the human body is an active area of research. In particular the relationship between arterial diseases like atherosclerosis and fluid mechanics has been and is in focus. The aim of these studies is to establish an explanation as to why atherosclerotic lesions occur preferentially at certain locations in the arterial tree. Among the cellular components of the arterial wall, the endothelium has received most of the attention. This seems reasonable due to its strategic location, positioned between the flowing blood and the underlying vessel wall.

Several fluid mechanical parameters have been linked to the selective development of stenoses in the arterial tree. Fry (1968) showed that endothelial cells were permanently damaged if the wall shear stress (steady

flow) exceeded 40 Pa. This high shear stress level is not generally present in the healthy arterial system. However, during haemodialysis using an arterio-venous fistula, such shear stress levels do exist (Borg, 2000). Caro et al. (1971) associated atherogenesis with disturbed mass transfer at low shear stress regions where the flow is slow and convective mass transfer is impaired. Ku et al. (1985) showed that plaque formation in the carotid bifurcation correlates well with low but oscillating shear stress. Complementary hypotheses have been provided more recently, which include effects of temporal and spatial gradients in the flow. In particular, large spatial variations of the wall shear stress occur at bends and bifurcations where spatial gradients normally are large. It has been shown that endothelial permeability to macromolecules like albumin depends on the wall shear stress level (Jo et al., 1991) and on the wall shear stress gradient by Phelps and DePaola (2000). High frequency fluctuations in wall shear stress make the wall more distensible (Roach, 1963).

* Corresponding author.

E-mail address: laszlo.fuchs@vok.lth.se (L. Fuchs).

During haemodialysis nearly all of the above factors are present in the neighborhood of the cannula. Depending on the flow rate in the cannula (speed of dialysis) the flow may be laminar or transitional-turbulent. Regions of high wall shear stress (close to 40 Pa) exist on the vein wall around the cannula and on the wall where the cannula jet impacts on the curved vein wall (Borg, 2000). Regions of permanently low shear stress and/or high shear stress gradients exist close to the cannula. For the highest flow rates possible in vivo high frequency oscillations in wall shear stress, and high Reynolds stresses in the interior of the flow exist (Borg, 2000).

Recently, it has been discovered that certain salt precipitation is present in stenotic AV fistulas (arterio-venous fistulas). These deposits are present only in stenotic AV fistulas and not in non-stenotic fistulas, nor in stenotic lesions that occur at other places in the arterial tree (Olsson, 2000).

Here, we report some results that reveal the appearance of solvent inhomogeneity in the blood. This inhomogeneity is the result of the streams from the cannula and the base flow in the vein. This concentration inhomogeneity interacts with the above-mentioned factors that are assumed to trigger the development of a venous stenosis. The mixing of a substance that is in excess in the stream from the cannula is studied experimentally using laser induced fluorescence (LIF) in an in vitro setup. The effects of the flow rates in the cannula and the vein, and the position of the cannula on the mixing patterns, are reported. Some complementary numerical simulations show good qualitative agreement with the LIF data.

2. Methods

The experimental setup is aimed to mimic the flow conditions around a real cannula. The geometry is therefore a somewhat simplified up-scaled version of a real cannula. The real cannula has an inner diameter of 1.8 mm and an outer diameter of 2.0 mm. The veins at the arm after the fistula have a diameter of 2–5 mm but vary significantly from one patient to another. The flow in the fistula is almost steady and therefore, we consider primarily steady-state situations. The rig is scaled such that it approximately corresponds to a real vein segment with an inner diameter of 4.3 mm. The angle between the vein and the cannula is fixed to 10°. Two different positions of the cannula are considered. In the first position, O1 the cannula tip is positioned 1 mm above the vein floor. A schematic picture of the vein and the cannula in position O1 is provided in Fig. 1. In the second position, named O2 the cannula is rotated 180° around its axis compared to configuration O1. Reference values for the flow rate through the real vein and the cannula are 0.26 and 0.60 l/min respectively. The

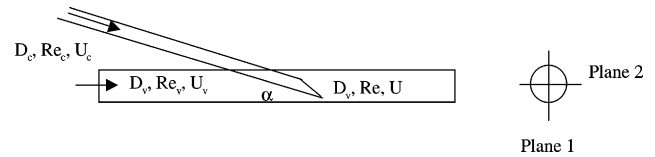


Fig. 1. Schematic picture of the cannula puncturing the vein. The subscripts c and v denote the cannula and the vein sides, respectively.

flow rate through the fistula is then 0.86 l/min (0.26 + 0.60 l/min). Assuming a viscosity of whole blood of 4×10^{-3} kg/m s and a density of 1000 kg/m³, the bulk Reynolds number in the cannula is 760, 740 in the vein and 1060 in the vein downstream of the cannula. These are reference values and we have varied the flow parameters around these values.

The concentration of a substance downstream of the cannula is expected to follow the functional relationship:

$$c = f(x, y, z, D_c, D_v, U_c, U, \alpha, \rho, \mu, D, C_c, C_v)$$

Here, c is the concentration of the substance, x , y and z denote the Cartesian coordinates, D_c is the diameter of the cannula, D_v is the diameter of the vein, U_c is the mean velocity in the cannula. U is the mean velocity in the vein downstream of the cannula, α is the angle between the cannula and the vein, ρ is the density of the fluid, μ is the viscosity of the fluid. D is the diffusivity of the passive scalar. C_c and C_v are the concentrations of the passive scalar in the two streams. Using dimensional analysis with U , ρ , and D_v as the reduction variables the following relation is obtained:

$$c = \Pi \left(\frac{x}{D_v}, \frac{y}{D_v}, \frac{z}{D_v}, \frac{D_c}{D_v}, Re, \frac{U_c}{U_v}, \alpha, Pe, C_c, C_v \right)$$

where Re is the Reynolds number and Pe is the Peclet number, given by:

$$Re = \frac{UD_v\rho}{\mu}, \quad Pe = \frac{UD_v}{D}$$

2.1. Investigated cases

The cases that has been investigated are summarized in Table 1. The table states also the ratio between mean axial velocity in the cannula and mean axial velocity in the vein (U_c/U_v). For large values of this ratio the flow behaves as a jet, causing stronger mixing. For high enough values the mixing layer becomes unstable (e.g. Cases 3 and 4).

2.2. Experimental setup

The experimental setup consist of two pumps and two elevated tanks which provide the necessary head to drive the flow through the model vein and cannula. The model of the vein is made of glass and has an inner diameter of 22 mm. The model of the cannula is made of plexiglass

Table 1
Parameter values of the cases considered in this study

Case	A	B	C
	$U_c/U = 1.15$	$U_c/U = 1.73$	$U_c/U = 2.30$
	$U_c/U_v = 1.44$	$U_c/U_v = 2.47$	$U_c/U_v = 3.84$
1	$Re = 409$ $Re_c = 196$ $Re_v = 327$	$Re = 409$ $Re_c = 295$ $Re_v = 286$	$Re = 409$ $Re_c = 393$ $Re_v = 246$
2	$Re = 818$ $Re_c = 393$ $Re_v = 655$	$Re = 818$ $Re_c = 589$ $Re_v = 573$	$Re = 818$ $Re_c = 786$ $Re_v = 491$
3	$Re = 1310$ $Re_c = 629$ $Re_v = 1048$	$Re = 1310$ $Re_c = 943$ $Re_v = 917$	$Re = 1310$ $Re_c = 1258$ $Re_v = 786$
4		$Re = 1638$ $Re_c = 1179$ $Re_v = 1146$	

and has an inner diameter of 9 mm and an outer diameter of 13 mm. The length of the model of the vein is 2.5 m before the cannula is inserted into the stream which assures a fully developed laminar profile before the insertion point. The length of the cannula is 0.5 m, which also assures a nearly developed flow for the Reynolds numbers considered. The working fluid is water with a temperature of 293 ± 3 K. To quantify mixing we use Rhodamine B in combination with a pulsed Nd:YAG laser. Rhodamine B is an organic molecule and has a strong fluorescence centered on the red–orange part of the visible spectrum. The maximum absorption of Rhodamine B occurs around 540 nm, which is close to the wavelength of the Nd:YAG laser (532 nm). To reduce refraction index errors the measurement section is submerged in a water-filled plexiglass box. The imaging system consists of a cross-correlation 1280×1024 pixel CCD camera (PCO SensiCam Double Shutter) with Nikon Micro-Nikkor 60-mm f/2.8 lenses. The scattered laser light is filtered out from the laser wavelength light using an optical filter (Kodak Wratten No. 22). A dual head Nd:YAG laser (Continuum Minilite PIV) of 2×25 mJ is used for illumination. Light sheet optics forms the laser beam to a light sheet. The light sheet is cut by a slit, reducing the laser sheet thickness to 0.5 mm. The timing of the system is controlled by a PC using software from La Vision. The same system has been used for DPIV measurements of the same flow.

2.3. LIF measurements

In the following, we give a short description for the quantitative concentration measurements. The description here is limited to low concentrations, lying in the linear range. A more general description is provided in Van Cruyningen et al. (1990). For fixed optical settings in the linear range the following simplified equation

holds for the digital signal level $i_d(x, y, n)$ in each pixel of the camera array for each laser pulse:

$$i_d(x, y, n) = k(x, y, n)c(x, y) + i_{db}(x, y, n) \quad (1)$$

In this equation $k(x, y, n)$ includes variations in laser energy over the sheet for pulse n and optical factors. $i_{db}(x, y, n)$ is the background fluctuations for zero concentration. We introduce the variable $i_{dc} = i_d - i_{db}$, that is the digital signal level with the local background subtracted and the following equation is obtained:

$$i_{dc}(n) = k(n)c \quad (2)$$

Note that the coordinates have been dropped in (2). We apply the same procedure for each pixel in the CCD array. We assume that fluctuations in laser energy and local background are so small that a reasonable estimate of k can be obtained by averaging over N pulses:

$$I_{dc} = Kc \quad \text{or} \quad \frac{1}{N} \sum_{i=1}^N i_{dc}(i) = \left(\frac{1}{N} \sum_{i=1}^N k(i) \right) c \quad (3)$$

To determine the constant K in each pixel, least square minimization is carried out over M tested concentrations in the assumed linear range resulting in the following estimate for K :

$$\hat{K} = \frac{\sum_{i=1}^M I_{dc}(i)c(i)}{\sum_{i=1}^M c(i)c(i)} \quad (4)$$

Confidence intervals for K , are given by:

$$K = \hat{K} \pm t_{m-2} \frac{s}{\sqrt{\sum_{i=1}^M (c(i) - \bar{c})^2}} \quad (5)$$

$$s = \sqrt{\frac{1}{M-2} \sum_{i=1}^M (I_{dc}(i) - Kc(i))^2}$$

In these equations the overbar denotes mean value and t_{m-2} is the t -distribution for M samples. With the help of this equation, the accuracy of the fit can be determined in each point in the pixel array. Typical values for the uncertainty of K is 5% in the current application. The fluctuations in the background are characterized by the standard deviation taken as 20–30 samples of images with the laser running, but no tracer in the system. In each point, we can estimate the total relative uncertainty by:

$$\varepsilon = \sqrt{(\varepsilon_K)^2 + (\varepsilon_{\text{laser}})^2 + (\varepsilon_{\text{bg}})^2} \quad (6)$$

where the first term under the root is the relative uncertainty in the linear regression, the second is the relative uncertainty due to fluctuations in laser energy and the last is due to fluctuations in the background. The background error determines the lowest concentration that can be measured with any accuracy. Typical values for the error in the current application are 5% relative error in K , 2.5% error due to laser fluctuations and 1%

error due to background fluctuations. In the measurements presented in this paper the mean relative error in the instantaneous concentration measurement is 6% and the maximum error is 10%. This holds for concentrations down to 6% of the inlet concentration. In regions with very low concentration, the relative error increases due to fluctuations in the background but the absolute error remains low.

3. Results

The results are presented in terms of mixing patterns in Planes 1 and 2 (c.f. Fig. 1) for the two different positions of the cannula O1 and O2. As outlined in Table 1, 10 different cases are investigated. For the Cases denoted by A, B and C the velocity ratio of the flow in the cannula and the vein, respectively, is kept constant. For a specific case number the Reynolds number in the vein downstream of the cannula is kept constant. We start by looking at results for mixing patterns in Plane 1. In Fig. 2 instantaneous mixing patterns for position O1 of the cannula are shown. The image plane extends from the cannula tip to four diameters downstream of the cannula tip. The pictures show gray scales of normalized concentration. For Cases 1A–1C, the flow and mixing patterns are laminar. We note that the region of high concentration near the vein floor extends over an increased distance when the cannula to vein velocity ratio increases. This is partly due to an increased momentum of the cannula jet and partly due to weaker compression of the jet by the rotational motion of the flow in the vein induced by the cannula. Numerical simulations of Cases 1A–2C show that two pairs of counter rotating vortices are set up behind the cannula. The strength of these vortices decreases as we move from Cases A to C. When the Reynolds number is increased to 818 (Fig. 2, Cases 2A–2C) the mixing patterns remains approximately the same as for Cases 1A–1C. We note that in Case 2C weak signs of transition are seen in the form of small blobs of high concentration. Similar structures are seen in Case 3A but now in the interior of the flow and further downstream. In Cases 3B, 3C and 4B the instability appears early in the cannula jet shear layer.

Velocity measurements made by DPIV on Case 4B show that in this case the wall jet downstream of the cannula has a width that is small compared to the radius of the vein. In the region where it starts to interact with the lower vein wall, we can consider it as approximately plane. Furthermore, the jet transverse velocity in this region is small although it increases quite rapidly as one moves away from the wall region. We have calculated the second derivative of the axial velocity in the transverse direction for this case, which shows that the jet profile has an inflection point. Around one vein diameter downstream of the cannula tip the upper side of the

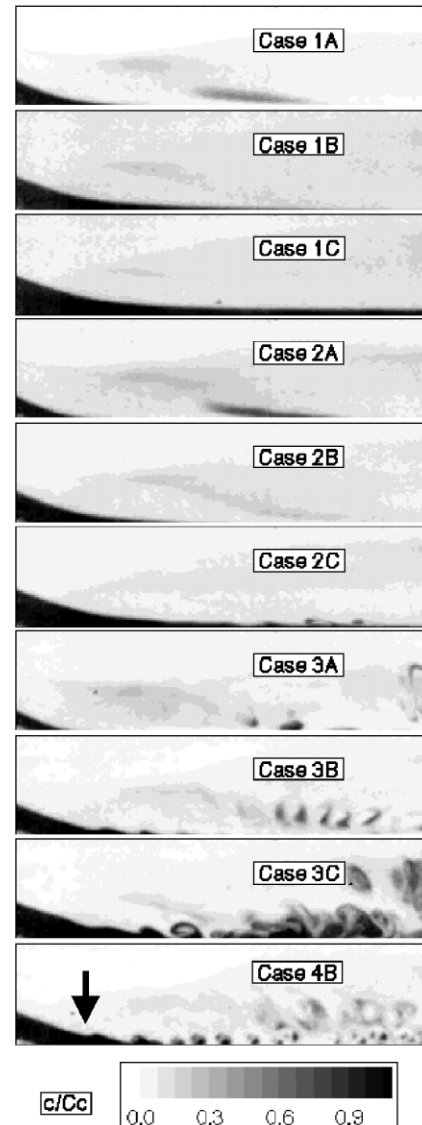


Fig. 2. Instantaneous mixing patterns in Plane 1 for position O1 of the cannula. The scale in the bottom of the figure shows the level of the relative concentration, c/C_c . The arrow in the lowest picture marks the tip of the cannula.

wall jet is well approximated by $u = a + b \cosh^2((y - y_0)/\delta)$ where y_0 is the center of the plane jet. The shear layer width is $\delta = 0.05D_v$ at this position and the distance between the vortices leading to the mixing patterns in Case 4B is 6δ . This is fairly close to the wavelength of the mode with maximum amplification rate for a high Reynolds number Bickley jet ($u = b/\cosh^2((y - y_0)/\delta)$) given by Lesieur (1997) which is 6.55δ .

Fig. 3 depicts the corresponding mixing patterns for the case when the cannula is rotated around its axis (Position O2). The secondary flow induced behind the cannula is weaker in this case than for position O1. Therefore, the jet is less compressed compared to position O1. As for Position O1, Case 1A, B and C remains laminar. Also here signs of transition are seen in



Fig. 3. Instantaneous mixing patterns in Plane 1 for Position O2 of the rotated (90°) cannula.

Case 2C and more expressed in 3A–3C. Fig. 4 depicts a comparison of the mixing with “normal” and rotated (180°) cannula. As seen, the cases with rotated cannula exhibit less mixing due to the weaker shear layer in that

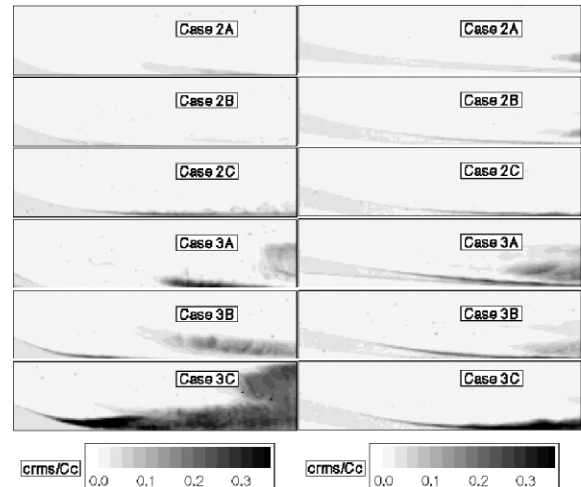


Fig. 5. Concentration fluctuations in Plane 1 at Positions O1 (left) and O2 (right) of the cannula. The gray scale shows the level of the relative concentration, c_{rms}/C_c .

case. Since it is so simple to rotate the cannula in clinical situations, it seems that one can affect the mixing by simple means. The clinical significance of this finding is to be studied in the future.

In Fig. 5 the corresponding fields of the fluctuations of the concentration (rms) in Plane 1 are depicted. The figures to the left correspond to Position O1 of the cannula and the ones to the right to Position O2. These figures quantify what is seen in the instantaneous pictures i.e. that fluctuations are nearly absent in Cases 2A and 2B, are weak in Case 2C and significant in Cases 3A–3C. Note the fast growth of instabilities in the jet shear layer in Case 3C, which leads to strongly enhanced mixing further downstream and high levels of concentration fluctuations close to the lower vein wall in the studied domain.

Instantaneous mixing patterns in Plane 2 for Position O1 of the cannula are presented in Fig. 6a. The images depict the plane from the cannula tip to 3.2 diameters

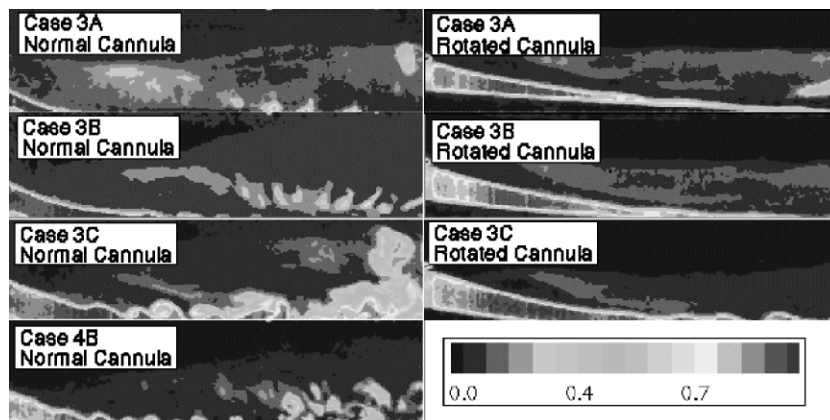


Fig. 4. Concentration fields with “normal” cannula and the corresponding rotated cannula by 90°.

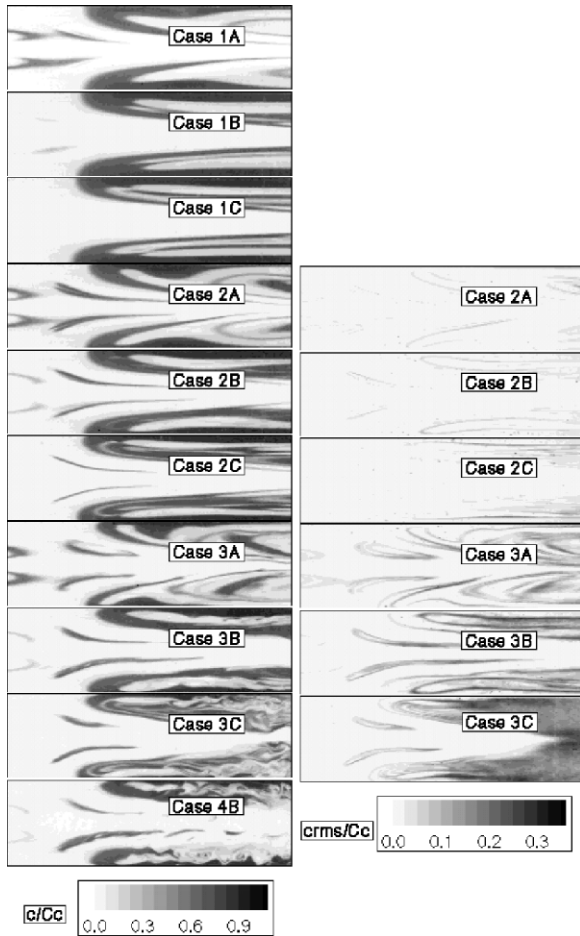


Fig. 6. The mixing patterns in Plane 2 for Position O1 of the cannula (6a, left). The corresponding rms fields of concentration fluctuations for Cases 2A–3C is given to the right (6b).

downstream of this position. The general behavior of the flow field is governed by the cannula jet that hits the lower vein wall and spreads along the vein wall, and the secondary flow induced by the jet. This leads to complicated mixing patterns even in the laminar cases which consist of long tiny structures of high concentration. We note that high concentration regions exist close to the vein walls for long distances downstream of the cannula in this plane. The formations of the patterns in Fig. 6a are easier to understand with the help of Fig. 7. This figure shows the mixing patterns in different cross-sections of the vein taken from numerical simulations for Case 1A and 1C. In this figure, we clearly see how the flow from the cannula hits the vein wall and spreads up along the vein walls as one moves downstream. For the higher Reynolds number cases we see that the elongated structures break down and small scale mixing is visible, as seen in Fig. 6. The same figure depicts also the rms of the concentration fluctuations on Plane 2. For the Cases 2A–2C the fluctuations are weak in this plane and for Cases 3A and 3B, the fluctuations appear in narrow

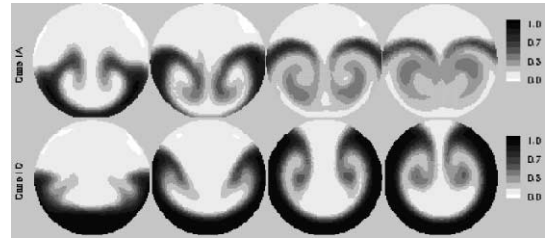


Fig. 7. Numerical simulation of the mixing patterns downstream of the cannula tip. Cannula Position O1. The position of the cross-sections are from left to right at $x/D_v = 1, 2, 4$ and 6 , where x is the coordinate from the cannula tip. The legend shows the level of c/C_c .

bands around the structures seen in Fig. 6a. We see that in Case 3C the concentration fluctuations are large in regions close to the vein wall and become more uniform in the plane as one moves downstream of the cannula tip.

4. Conclusions

The mixing around a model of a cannula puncturing a vein during haemodialysis have been studied for physiological flow rates. The flow parameters are varied so that they correspond to different flow rates through the fistula and different speeds of the dialysis.

The results show that the flow changes from laminar to transitional depending of these two parameters. The impact of this on the mixing patterns and the rms of the concentration fluctuations in the neighborhood of the cannula are shown. In the laminar cases, the concentration of the substance entering from the cannula remains high along parts of the vein wall for long distances downstream. For the higher Reynolds numbers the flow loses its stability leading to high frequency concentration fluctuations ($O(100)$ – $O(1000)$ Hz) close to the wall in the real application. The rms values of the concentration fluctuations close to the vein wall are high in those cases.

It has also been found that altering the orientation of the cannula leads to a significant change in the mixing pattern. The clinical significance of this finding has to be further studied.

References

- Borg, A., 2000. Experimental and numerical studies of flows related to the processes of atherosclerosis. ISRN LUTMDN/MVK-1022-SE, Ph.D. Thesis, Lund Institute of Technology, Sweden.
- Caro, C.G., Fitzgerald, J.M., Shroter, R.C., 1971. Atheroma and arterial wall shear observations, correlation and proposal of a shear dependent mass transfer mechanism for atherogenesis. Proc. R. Soc. London Sr. B 17 (7), 109–159.

- Fry, D.L., 1968. Acute vascular endothelial changes associated with increased blood velocity gradients. *Circ. Res.* 22, 165–197.
- Jo, H., Dull, R.O., Hollis, T.M., Tarbell, J.M., 1991. Endothelial albumin permeability is shear dependent, time dependent, and reversible. *Am. J. Physiol.* 269, H1992–H1996.
- Ku, D.N., Giddens, D.P., Zarins, K.Z., Glagov, S., 1985. Pulsatile flow and atherosclerosis in the human carotid bifurcation: positive correlation between plaque location and low and oscillating shear stress. *Atherosclerosis* 5, 293–302.
- Lesieur, M., 1997. *Turbulence in fluids*. Kluwer Academic Publishers, Dordrecht.
- Olsson, L.-F., 2000. Private Communication in August 2000. Gambro Research, Gambro AB, Lund, Sweden.
- Phelps, J.E., DePaola, N., 2000. Spatial variations in endothelial barrier function in disturbed flow in vitro. *Am. J. Physiol.* 278, H469–H476.
- Roach, M.R., 1963. An experimental study of the production and time course of poststenotic dilation in the femoral and carotid arteries of adult dogs. *Circ. Res.* 13, 537–551.
- Van Cruyningen, I., Lazano, A., Hanson, R.K., 1990. Quantitative imaging of concentration by planar laser-induced fluorescence. *Exp. Fluids* 10, 41–49.